Lightning parameters of sprites and diameter of halos over South Africa

D.C Mashao[1, 2], M.J Kosch[2, 3,4], M. Füllekrug[5], and J. Mlynarczyk[6]

[1]Department of Physics, University of KwaZulu-Natal, Durban 3629, South Africa

[2]South African National Space Agency, Hermanus 7200, South Africa

[3]Department of Physics, Lancaster University, Lancaster LA1 4YB, UK

[4]Department of Physics, University of Western Cape, Bellville 7535, South Africa

[5]Department of Electronic and Electrical Engineering, University of Bath, Bath BA2 7AY, UK

[6]Institute of Electronics, AGH University of Science and Technology, Krakow 30-059, Poland

Corresponding author: Dakalo Mashao (mashaodakalo@gmail.com)

Abstract

Transient Luminous Events (TLEs) above thunderclouds have been previously associated with variables such as the lightning Charge Moment Change (CMC), charge height, charge transfer, and lightning current rise-time. We show for the first time a comparison of the CMC, rise-time, fall-time, peak electric field, and peak current of the lightning discharges associated with 11 column, 11 carrot, and 18 sprites with halo. We found that carrot sprites are induced by a lightning discharge with CMC, peak electric field, and peak current greater and less than that for column sprites and sprites with halo, respectively. Sprites with a halo are initiated by a lightning discharge with a longer rise-time and fall-time than that for column and carrot sprites. Column sprites top altitude and carrot sprites brightest region altitude positively correlate with lightning rise-time. For carrot sprites top altitude, the results suggest that the electrical breakdown region decreases in altitude for a longer fall-time, greater peak electric field, and greater peak current. For the altitude of the sprites brightest region, column sprites correlate negatively with lightning fall-time, peak electric field, and CMC, and column sprites top altitude also correlates negatively with lightning peak electric field. For sprites with a halo top altitude increased with lightning fall-time and peak current, and sprites with a halo brightest altitude increased with an increase in lightning CMC. Halo diameters correlate positively with lightning fall-time, peak electric field, and peak current.

The investigated lightning parameters can be used to identify the initiated sprites morphological type when optics are not available.

Keywords: Lightning rise-time; lightning fall-time; lightning Charge Moment Change; Lightning electric field; Lightning current; Transient Luminous Events altitude

1. Introduction

Sprites are vertically oriented luminous electric discharges induced by the cloud-to-ground (CG) lightning quasi-static electric field and continuing current. They appear at stratospheric and mesospheric altitudes of about 40 to 100 km (Füllekrug et al., 2006; Liu et al., 2015; Pasko, 2010; Pasko et al., 2013; Siingh et al., 2012; Surkov and Hayakawa, 2020). In contrast, halos manifest as a cone of luminous emission, also generated by the CG lightning quasi-static electric field and continuing current, at ionospheric altitudes of about 85 km. The duration of the electric field at a certain altitude is almost equivalent to the local Maxwellian relaxation time, which is defined as the permittivity of free space over the local conductivity. The local Maxwellian relaxation time increases with a decrease in atmospheric altitude (Liu et al., 2015; Pasko et al., 1997).

Sprites and halos are induced by mainly positive CG lightning electric fields, although some are generated by negative CG lightning discharge. Sprite streamers tend to develop from halos (Luque & Ebert, 2009). Column sprites are associated with only the downwards propagation of streamers, whereas carrot sprites are associated with both downwards and upwards streamer propagation (Bór, 2013). The Transient Luminous Events (TLE) manifest themselves about 1—100 ms after the parent CG lightning flash. (Bering et al., 2004; Chen et al., 2019; Frey et al., 2007; Liu et al., 2015; McHarg et al., 2002; Siingh et al., 2012; Williams et al., 2012). The parent lightning waveforms are shorter than the duration of the TLE luminosity.

Parameters such as lightning charge height, total charge transfer, rise-time, peak current, and Charge Moment Change (CMC) are essential in determining whether the lightning stroke initiates sprites or halos (Adachi et al., 2010; Asano et al., 2008; Yaniv et al., 2014; Haspel et al., 2020; Li et al., 2008; Mashao et al., 2021). Lightning with a mean and minimum CMC value of approximately 1480 C-km and 63 C-km has been associated with the generation of sprites (Chen et al., 2019). Enhancement in sprites brightness with an increase in lightning CMC has been reported by Cummer et al. (1998), Takahashi et al. (2010), Yaniv et al. (2014), Yang et al. (2017), and Nnadih et al. (2018). According to Yang et al. (2017), a

positive correlation exists between sprites vertical extent and lightning CMC. Adachi et al. (2004) found that the lightning CMC and peak current are proportional to the length of column sprites and the number of columns, respectively. Mashao et al. (2021) demonstrated a positive correlation between lightning CMC and sprites top altitude. The importance of lightning rise-time on sprites has been established by Asano et al. (2008) using a two-dimensional computer simulation for summer and winter storm conditions. According to Asano et al. (2008), lightning charge height, charge transfer, and rise-time are essential in the generation and development of sprites. The sprites breakdown region reduces in altitude for a longer rise-time (>25 μs) (Asano et al., 2008). We are not aware of any observational report of lightning fall-time regarding TLEs.

The altitudes of sprites have been well established using different techniques and high-speed cameras. The sprites top altitude has been observed to vary from 73 to 96 km, whereas the altitude of the sprites brightest region has been found to span from 50 to 84.1 km (Füllekrug et al., 2019; Luque et al., 2016; Mashao et al., 2021 Malagón-Romero et al., 2020; Sentman et al.,1995; Stenbaek-Nielsen et al., 2010; Wescott et al., 1998). Mashao et al. (2021) found that the average sprites top altitude in South Africa occurred at approximately 84.3 km. Other authors found sprite top altitudes at 88 km (Sentman et al., 1995), 86.4 km (Wescott et al., 1998), and 79-96 km (Stenbaek-Nielsen et al., 2010). Mashao et al. (2021) found that the average altitude of maximum brightness in South Africa occurred at approximately 69 km. Other authors found the altitude of maximum brightness at 70 km (Malagon-Romero et al., 2020) and 71.2-72.4 km (Luque et al., 2016). Wescott et al. (2001) observed that the top altitude of sprites with halos varied from 73.5 km to 85.2 km, with an apparent diameter of about 66 km. Taylor et al. (2008) found a diameter of about 89± 5 km for a negative CG sprite with a halo. According to Miyasato et al. (2002), the average halo diameter was about 86 km.

In this paper, we demonstrate the importance of lightning CMC, peak electric field, peak current, rise-time, and fall-time (for the first time) on sprites altitude and halo diameters for different sprites morphologies observed over South Africa. This is done by evaluating the linear correlation between lightning CMC, peak electric field, peak current, rise-time, and fall-time versus the top altitude and altitude of the brightest region of column sprites, carrot sprites, and any sprites with halos. In addition, we measure the diameter of halos in South Africa for the first time.

2. Observations

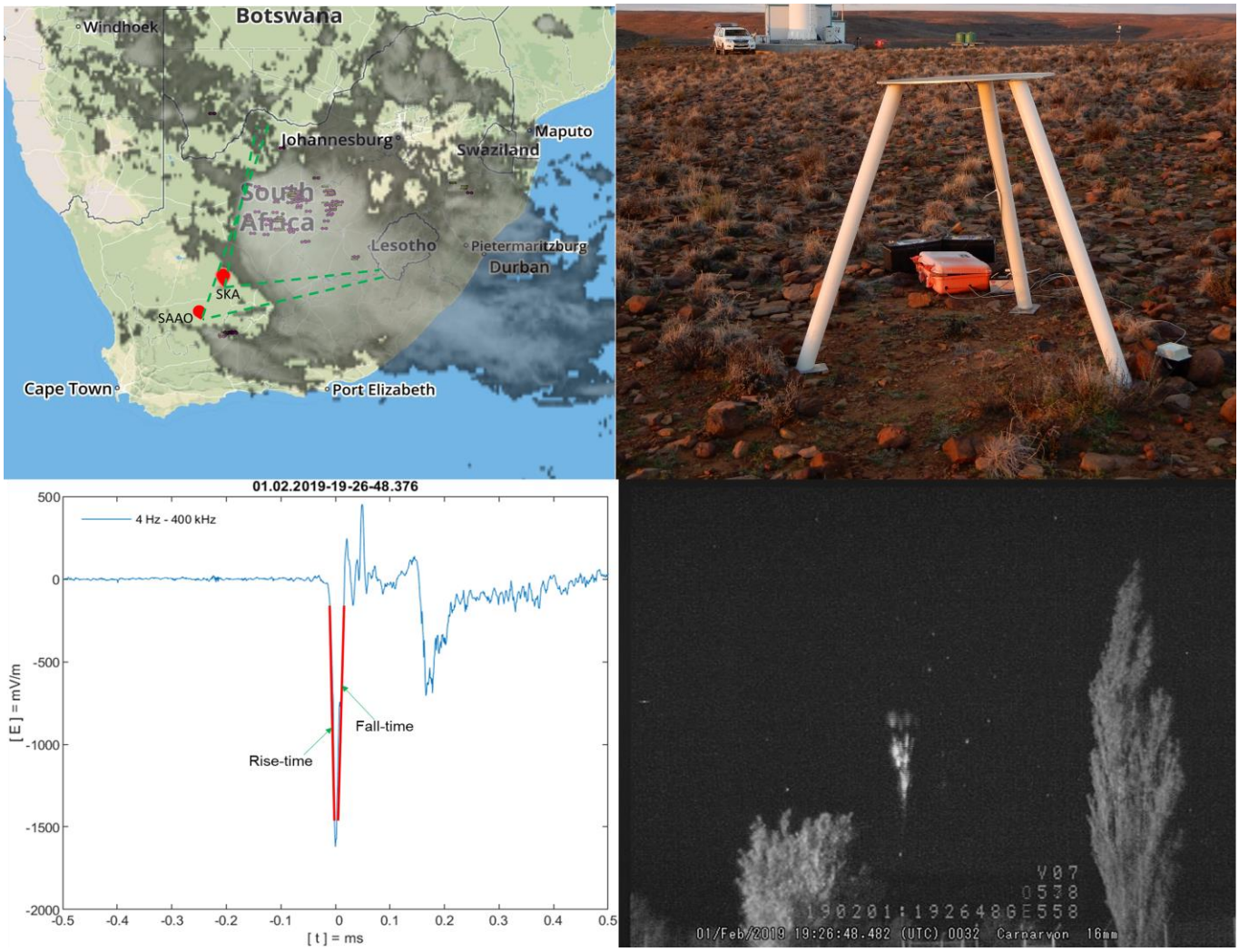

Fig. 1. South African map (top left panel, obtained from EarthNetworks) denoting the thunderstorm which initiated some of the TLEs in this paper and observation sites (red dots) of the South African Astronomical Observatory (SAAO) and Square Kilometre Array (SKA) in the Northern Cape, South Africa. The green dotted lines show camera viewing directions. The yellow plus, yellow negative, and pink dash-like symbols denote the positive CG, negative CG, and intracloud lightning, respectively. Lightning vertical electric field (bottom left panel) associated with a carrot sprite (bottom right panel) measured by the ELF receiver (4 Hz- 400 kHz) (top right panel). The red lines (bottom left panel) indicate where the rise-time and fall-time were calculated from 90% to 10% of the maximum electric field signal deflection from the background. A carrot sprite recorded on 01 February 2019 at 19:26:48.558 UTC (bottom right panel) using a Watec 910Hx camera.

2.1 Camera systems

The TLEs presented here were recorded using Watec 910Hx cameras (Bór, 2013; Gamerota et al., 2011; Liu et al., 2016; Soula et al., 2009; Stenbaek-Nielsen et al., 2010; Vadislavsky et al. 2009; Yaniv et al., 2014) over South Africa. Fig. 1 (top left panel) shows two distinct locations; the Square Kilometre Array (SKA) (30.97º S, 21.98º E) and the South African

Astronomical Observatory (SAAO) (32.38º S, 20.81º E), where the Watec 910Hx cameras were operated. Both locations are in the Karroo desert of the Northern Cape of South Africa, see Fig. 1 (top left panel).

The Watec 910Hx cameras had a 8.0 mm f/1.4 C-mount lens, giving a field of view (FOV) of 46.2º horizontal and 29º vertical. The Watec 910Hx cameras operated under fixed gain and a gamma factor of 0.45. The observation systems recorded sprites video clips at 25 fps with a 40 ms frame period. A GPS video timer installed in one camera system provided millisecond timing. A Network Timing Protocol server provided timing accuracy of about 1 ms for the other camera systems at SKA and SAAO. The camera systems operated with 8-bit intensity resolution. The video images had a size of 640x480 pixels with an angular resolution of 0.072º horizontal and 0.061º vertical per pixel. Thus, 1 pixel is 0.061º in elevation angle.

The 2019 sprites campaign was conducted from 28 January to 15 February 2019. Several Mesoscale Convection Systems (MCS) initiated the TLEs, moving from the northwest to the southeast over South Africa on 29 and 30 January as well as 1, 2, and 11 February 2019. The MCS produce TLEs for about 4 hours on average each night. Fig. 1 (top left panel) shows one MCS that induced the observed TLEs events (https://www.earthnetworks.com/product/decision-support-collaboration-tools/sferic-maps/). The 40 TLEs presented here were recorded on 29, 30 January and 11 February 2019 from SAAO and 1 and 2 February 2019 from SKA. Fig. 1 (bottom right panel) shows an example carrot sprite observed from SKA on 1 February 2019. Out of about 208 TLEs, 40 TLEs consisting of 11 column, 11 carrot, and 18 sprites with halos were selected for our analysis. We selected the TLEs that only contain column, carrot, and sprites with a halo to make a fair parent lightning parameters comparison. However, sprites with a halo consist of column, carrot, wishbone, and jellyfish sprites.

2.2 Altitude estimation

The stars in the sprites image background allowed us to determine the azimuth and elevation angle of every pixel. The star declination and right ascension from the star almanac, event time, and observation site were used to fit the modeled stars onto the real stars in the sprites image background in order to find the camera pointing direction and FOV, and to determine the azimuth and elevation angle of each pixel. To estimate the altitude of sprites, we assumed that sprites were induced directly above their parent CG lightning strokes. This supposition is usually used in TLEs studies (Füllekrug et al., 2019; Li et al., 2008; Luque et al., 2016;

Mashao et al., 2021; McHarg et al., 2007). However, there are reports of TLEs not induced directly above their parent lightning strokes with horizontal displacement up to about 150 km (Bór et al., 2018; Haspel et al., 2020, 2022; Füllekrug et al., 2001; Mashao et al., 2022; Mlynarczyk et al., 2015; Sao-Sabbas et al., 2003; Wang et al., 2019). The sprites altitude was estimated from their elevation angle and ground distance from the observation location. This was done by employing planar trigonometry in the vertical plane and spherical trigonometry in the horizontal plane. The method is fully described in Mashao et al. (2021). The altitude of sprites uncertainty, which depends on the slant distance between observation location and targeted sprites altitude, spanned ±0.33-0.47 km.

The sprites altitudes were estimated for two regions: the top altitude and the altitude of the brightest region. For a vertical profile through each TLE, the top altitude is the highest elevation angle pixel with an intensity value greater than the background. The diameter of the halos is determined in the same way for a horizontal profile. The altitude of maximum brightest is taken from the pixel of greatest intensity value within the TLE. The sprite top altitude is where electric field energy within a sprite is less than the altitude dependent critical breakdown field. The brightest region is where photon production maximizes due to collisions between the accelerated electrons and background neutrals (Liu et al., 2015; Mashao et al., 2021).

2.3 Lightning detection

We obtained the lightning information (time, position, peak current) of the TLEs parent CG lightning strokes from the South African Weather Service (SAWS) and Earth Networks (EN) (Gijben, 2012; Zhu et al., 2017). The parent CG lightning strokes were located between 242 and 707.5 km away from the observation sites, so well within the maximum observing range (900 km). The parent lightning strokes were all of the positive polarity with a peak current spanning from 32 to 179 kA. Based on timing data, SAWS and EN did not detect all lightning discharges which initiated the TLEs. This limited the number of TLEs to report.

2.4 Electromagnetic Waveforms

A wideband digital ELF radio receiver, co-located with the cameras, detected the lightning vertical electric field strength associated with the optical sprites in the frequency range from ~4 Hz to ~400 kHz with a sampling frequency of 1 MHz and timing accuracy of 12 ns (see Fig. 1, top right panel) (Füllekrug, 2010). The ELF radio receiver was positioned in a low radio interference area near the SKA site. The TLEs parent lightning electric field strength

span 1.0-3.8 V/m at the ELF radio receiver location. The lightning electric radiated fields propagate as $^{1}/_{r^2}$, where *r* is the distance from the lightning location to the receiver location (Cooray and Lobato, 2020). For comparison, we normalized the lightning peak electric field values for the distance from the ELF receiver to the lightning stroke location. This was done by multiplying the lightning peak electric field values by the distance squared (in km) relative to 1 km (Taylor and Jean, 1959). The lightning rise-time and fall-time were computed from the vertical electric field measured simultaneously with the optical observations (Füllekrug, 2010; Füllekrug et al., 2019). The rise-time calculations were from 90% to 10% of the maximum electric field signal deflection from background. The same method was applied to the fall-time (see Fig. 1, bottom left panel).

The lightning CMC values ranged from 689 to 6,780 C-km and were computed from the far-field magnetic field data recorded by a broadband ELF system installed in the Bieszczady mountains in Poland (49.20º N, 22.54º E), using the method described by Mlynarczyk et al. (2015). The ELF system measures the two horizontal magnetic field components in the frequency range from 0.01 to 1,000 Hz with a sampling frequency of 3 kHz (Mlynarczyk et al., 2018). The electromagnetic waves in the ELF range propagate in the Earth-ionosphere waveguide. The ELF propagation is unimodal and the attenuation rate is extremely low: at 30 Hz, for example, it is roughly 0.6 dB/Mm. The attenuation rate versus frequency for the daytime and nighttime ionosphere can be seen in Figure 3 of Kulak and Mlynarczyk (2011). These features of the ELF propagation allowed us to obtain a high signal-to-noise ratio in the magnetic field recordings from the northern hemisphere used in this study. It is also worth noting that the calibration of our equipment is also regularly controlled (Kulak and Mlynarczyk, 2011). Due to signal noise and unknown locations of the parent lightning strokes, we could compute the lightning CMC for only 31 TLEs, see Table 1 in the appendix.

All data are summarized in Table 1 in the appendix.

3. Results and discussions

An analysis of lightning rise-time, fall-time, peak electric field, peak current, and CMC associated with TLEs was conducted on 11 column sprites, 11 carrot sprites, and 18 any sprites with halos observed over South Africa. Note that the sprites with halos have different morphologies, i.e., column, carrot, wishbone, and jellyfish.

The lightning normalized peak electric field, peak current, rise-time, fall-time, and CMC associated with the analyzed TLEs vary from 93 to 914 kV/m, 32 to 179 kA, 6 to 25 µs, 1 to

91 μs, and 689 to 6,780 C-km, respectively. Most of the investigated TLEs producing parent lightning had a very short rise-time (<15 μs) and short fall-time (<25 μs); see Table 1. We found that TLEs top altitudes vary from 71 to 90.5 km, with an average and standard deviation of 79.8 and 5.2 km, respectively. The TLEs top altitudes are in the altitude range previously reported in the literature (Füllekrug et al., 2019; Luque et al., 2016; Mashao et al., 2021 Malagón-Romero et al., 2020; Sentman et al.,1995; Stenbaek-Nielsen et al., 2010; Wescott et al., 1998). The analyzed TLEs brightest region altitude ranged from 50 to 73 km, with an average and standard deviation of 61.5 and 6.4 km, respectively. The TLEs altitudes of maximum brightness are in the altitude range reported in the literature (Füllekrug et al., 2019; Luque et al., 2016; Mashao et al., 2021 Malagón-Romero et al., 2020; Sentman et al.,1995; Stenbaek-Nielsen et al., 2010; Wescott et al., 1998).

The top altitude for column sprites, carrot sprites, and sprites with halos (halo top) varied from 72.4 to 86.4 km, 70.7 to 87 km, and 71.5 to 90.5 km, respectively. We obtained an average top altitude for column sprites, carrot sprites, and sprites with halos of about 80.4 (±4.6), 80.6 (±5.1), and 78.9 km (±5.6 km), where the value in parenthesis is the standard deviation. The brightest region altitude for column sprites, carrot sprites, and sprites with halos ranged from 55.1 to 73 km, 50 to 68.5 km, and 50 to 68 km, respectively. The average altitude for column, carrot, and sprites with halos was 66 (±6.5), 61 (±5.5), and 59 (±5.2) km, where the value in parenthesis is the standard deviation.

The lightning normalized peak electric field, peak current, CMC, rise-time, and fall-time for column sprites ranged from 101 to 355 kV/m, 34 to 87 kA, 880 to 2,410 C-km, 7 to 16 μs, and 1 to 30 μs, respectively, with an average of 211 (74) kV/m, 48.5 (15.2) kA, 1,674 (583) C-km, 11.1 (2.8) μs, and 15.3 (8.1) μs, where the value in parentheses is the standard deviation. Carrot sprites were induced by lightning flashes with normalized peak electric field, peak current, CMC, rise-time, and fall-time varying from 93 to 427 kV/m, 32 to 92 kA, 1,360 to 3,060 C-km, 6 to 19 μs, and 1 to 32 μs, respectively, with an average of 233 (125) kV/m, 58 (17.4) kA, 2,187 (601) C-km, 11 (5) μs, and 15.6 (12.2) μs. The lightning normalized peak electric field, peak current, CMC, rise-time, and fall-time, which initiated any sprites with halos, had values ranging from 180 to 914 kV/m, 60 to 179 kA, 639 to 6,780 C-km, 8 to 25 μs, and from 10 to 91 μs, respectively, with an average of 519 (210) kV/m, 106.2 (30.6) kA, 2,909 (1,983) C-km, 12.8 (4.8) μs, and 36.3 (22.4) μs.

Clearly, column and carrot sprites require a less lightning CMC and smaller lightning rise-time and fall-time compared to any sprites with a halo. Sprites with halos require a

significantly greater lightning CMC and significantly longer lightning fall-time when compared to carrot and column sprites, as shown in Table 1. Column sprites require a lower lightning electric field and peak current compared to carrot sprites and sprites with a halo. The lightning discharges which initiate carrot sprites have a CMC, peak electric field, and peak current greater and less than that of the column sprites and sprites with halo, respectively.

We correlated the various lightning parameters against the brightest region and top altitude of column, carrot, and sprites with halo, and their relationships are presented below. According to Peat et al. (2009), Pearson's linear correlation coefficients spanning from 0.1 to 0.3 are small correlations, 0.3 to 0.5 are moderate correlations, and greater than 0.5 are high correlations.

3.1 Sprites top altitude

Fig. 2 shows the relationship between lightning fall-time (X, μs) (top left row), normalized peak electric field (E, kV/m) (top middle row), and peak current (I, kA) (top right row) versus the top altitude (Y, km) of carrot sprites. Fig. 2 also shows lightning rise-time (T, μs) (middle left row) and normalized peak electric field (E, kV/m) (middle center row) versus the top altitude (Y, km) of column sprites, as well as lightning fall-time (X, μs) (bottom left row) and peak current (I, kA) (bottom right row) versus top altitude (Y, km) of sprites with a halo. The Pearson correlation coefficient (r) and the linear fit equation (Y, km) are denoted on the top corner of each panel. The weak correlations between lightning CMC, rise-time, fall-time, peak electric field, and peak current against top altitude and brightest region altitude of column, carrot sprites and sprites with a halo, and as well as halo diameters are insignificant and therefore not presented here.

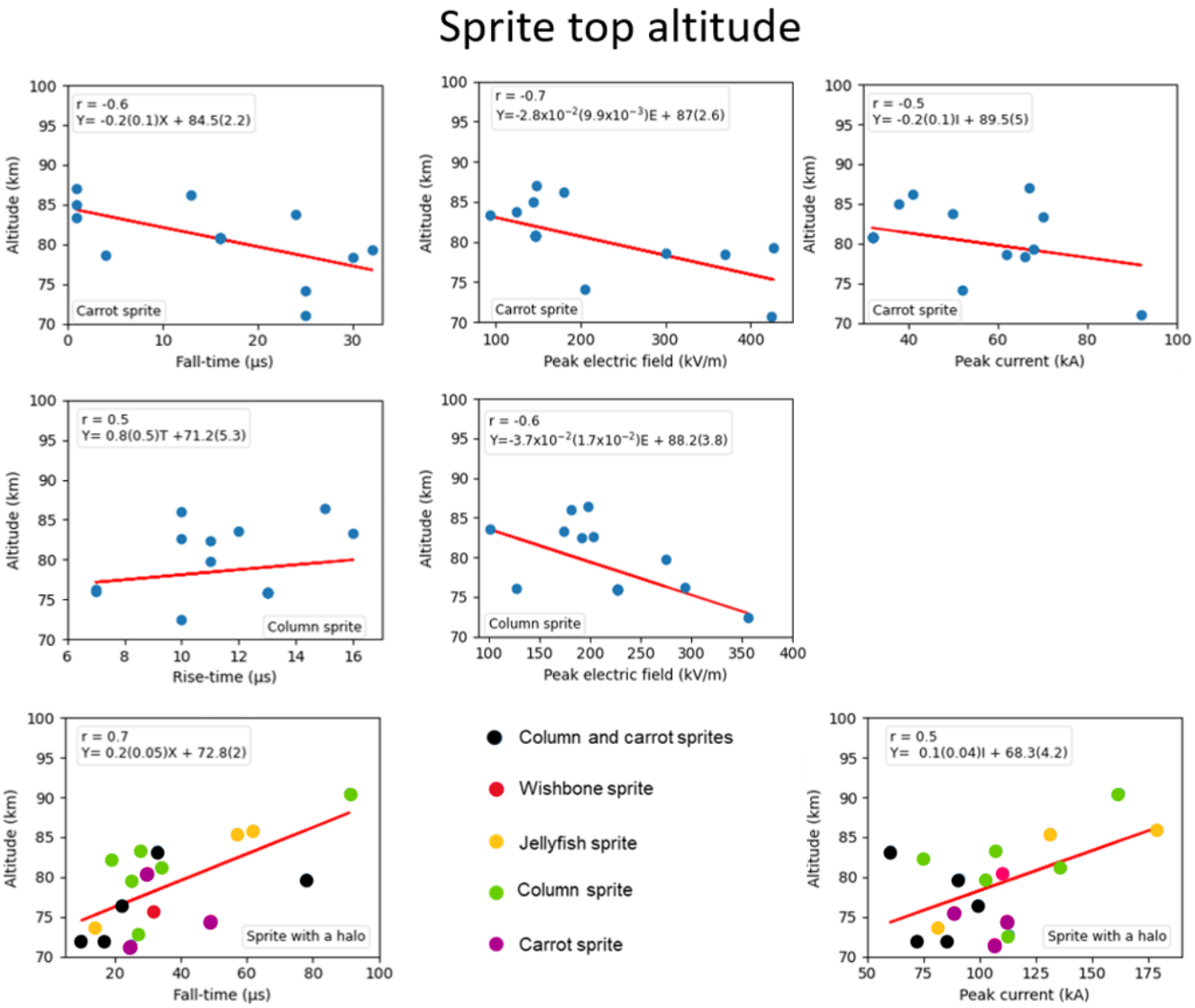

Fig. 2. Lightning fall-time (X, μs) (top left row), normalized peak electric field (E, kV/m) (top middle row), and peak current (I, kA) (top right row) versus the top altitude (Y, km) of carrot sprites. Lightning rise-time (T, μs) (middle left row) and normalized peak electric field (E, kV/m) (middle center row) versus the top altitude (Y, km) of column sprites. Lightning fall-time (X, μs) (bottom left row) and peak current (I, kA) (bottom right row) versus top altitude (Y, km) of sprites with a halo.). For sprite with a halo, different types of sprites are color-coded. The Pearson correlation coefficient (r) and the linear fit equation (Y, km) are denoted on the top corner of each panel. The value in parentheses in the linear fit equation is the uncertainty.

The top altitude of column sprites against lightning rise-time and peak electric field showed good positive and negative linear correlations (0.5) and (-0.6), respectively. The good positive (0.5) and weak negative (-0.2) (not shown) correlations found between the lightning rise-time and fall-time against the top altitude of column sprites, respectively, might be associated with the downward propagation of streamers and the lack of upward propagating streamers during column sprites initiation processes (Bór, 2013).

The top altitude of carrot sprites against lightning fall-time, peak electric field, and peak current showed good negative linear correlations (-0.6), (-0.7), and (-0.5), respectively. The top altitude of sprites with halos against lightning fall-time and peak current showed good positive linear correlations (0.7) and (0.5), respectively. For carrot sprites, this suggests that the electrical breakdown region decreases in altitude for a longer fall-time, greater peak electric field, and greater peak current.

3.2 Sprites brightest region altitude

Fig. 3 shows the relationship between lightning fall-time (X, μs) (top left row), normalized peak electric field (E, kV/m) (top middle row), and CMC (Z, C-km) (top right row) versus the altitude (Y, km) of the brightest region for column sprites. Fig. 3 also shows lightning rise-time (T, μs) (middle left row), normalized peak electric field (E, kV/m) (middle center row), fall-time (X, μs) (bottom left row), and peak current (I, kA) (bottom center row) versus the altitude (Y, km) of the brightest region for carrot sprites (middle row), as well as lightning CMC (Z, C-km) (bottom right row) versus the altitude (Y, km) of the brightest region for sprites with a halo (bottom row). The Pearson correlation coefficient (r) and the linear fit equation (Y, km) are denoted on the top corner of each panel.

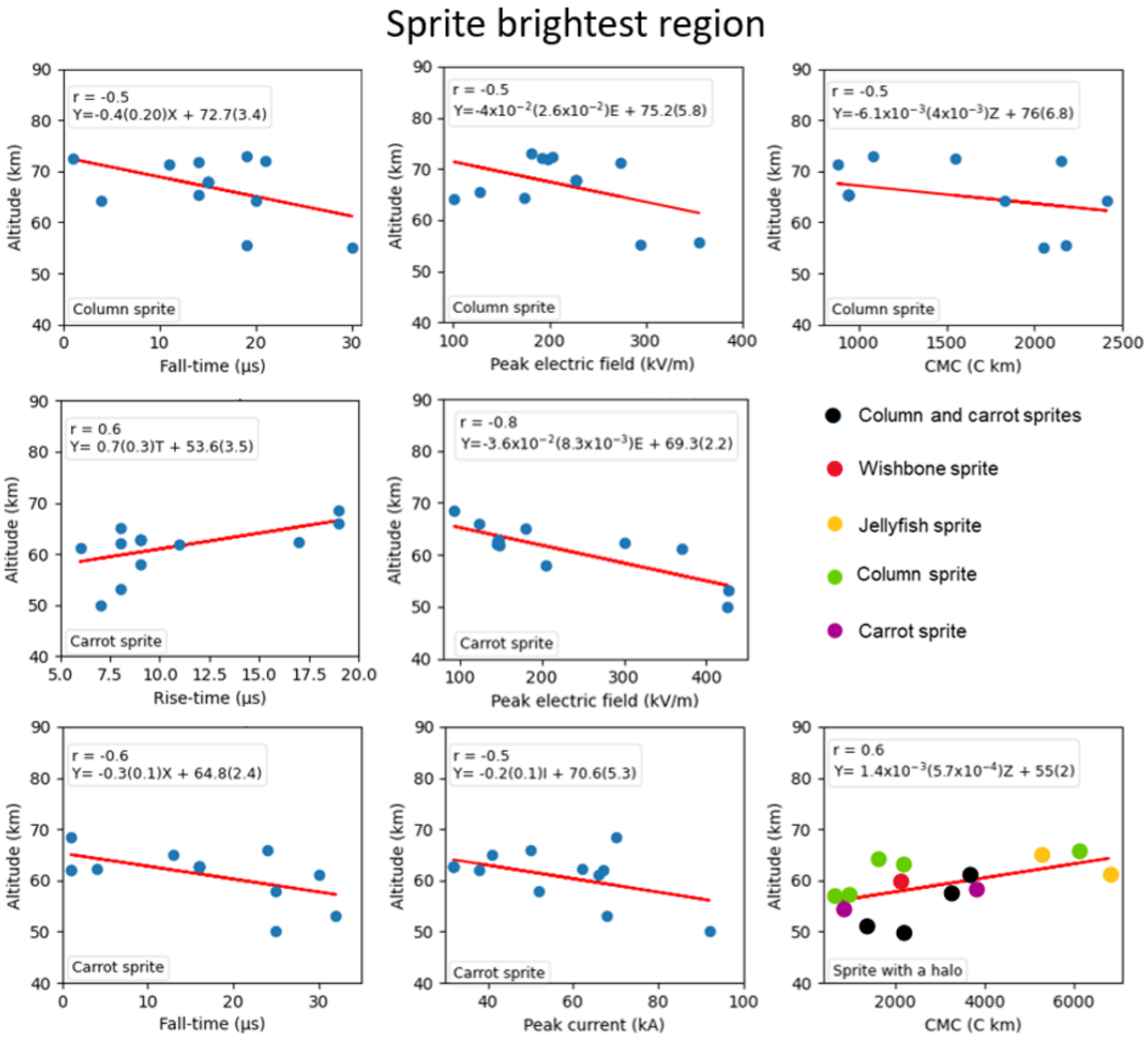

Fig. 3. Lightning fall-time (X, μs) (top left row), normalized peak electric field (E, kV/m) (top middle row), and CMC (Z, C-km) (top right row) versus the altitude (Y, km) of the brightest region for column sprites. Lightning rise-time (T, μs) (middle left row), normalized peak electric field (E, kV/m) (middle center row), fall-time (X, μs) (bottom left row), and peak current (I, kA) (bottom center row) versus the altitude (Y, km) of the brightest region for carrot sprites (middle and bottom row). Lightning CMC (Z, C-km) (bottom right row) versus the altitude (Y, km) of the brightest region for sprites with a halo (bottom right row). For sprite with a halo, different types of sprites are color-coded. The Pearson correlation coefficient (r) and the linear fit equation (Y, km) are denoted on the top corner of each panel. The value in parentheses in the linear fit equation is the uncertainty.

For column sprites, there are good negative correlations for the altitude of maximum brightness versus lightning fall-time (-0.5), peak electric field (-0.5), and CMC (-0.5). The

altitude of maximum brightness for carrot sprites shows a good positive correlation against lightning rise-time (0.6) and a good negative correlation against lightning peak electric field (-0.8), peak current (-0.5), and fall-time (-0.6). The good positive and negative correlation for carrot sprites against lightning rise-time and fall-time, respectively, might be related to the downward and upward propagation of streamers during carrot sprites initiation (Bór, 2013). On the other hand, for any sprites with halos, the altitude of maximum brightness has a good positive correlation with lightning CMC (0.6).

The results indicate that lightning with a longer fall-time, larger electric field, larger peak current, and larger CMC tend to deposit more energy at lower altitudes for column and carrot sprites, as shown in Fig. 3. However, lightning with larger CMC tends to deposit more energy at higher altitudes for sprites with a halo.

In addition, we have determined the vertical extent, the number of elements in each sprites event (e.g., number of columns), and maximum brightness of column and carrot sprites, and sprites with a halo. The maximum background subtracted brightness of sprites and sprites with a halo was obtained (see Nnadih et al. (2018)). For column sprites, the lightning CMC showed good positive correlation coefficients of 0.8, 0.9, and 0.8 against the number of columns in column sprites events, vertical extent, and maximum brightness of column sprites, respectively. The lightning CMC shows a good positive correlation coefficient of 0.5 against the maximum brightness of carrot sprites. These agree with Cummer et al. (1998), Takahashi et al. (2010), Yaniv et al. (2014), Yang et al. (2017), and Nnadih et al. (2018). However, we did not find a good correlation between lightning peak current and number of columns reported by Takahashi et al. (2010).

A good positive correlation coefficient of 0.5 exists between the lightning peak electric field and the maximum brightness of column sprites. The number of elements in carrot sprites events shows a good negative correlation coefficient of -0.7 against the lightning peak electric field. The negative correlation in carrot sprites events might be due to the existence of upward propagation of streamers processes which does not occur in column sprites formation processes (Bór et al., 2013). No good correlation was found between the vertical extent, number of sprite elements in sprites with a halo, and maximum brightness of sprites with a halo against any of the lightning parameters.

3.3 Sprites with a halo diameter

335 Fig. 4 shows the relationship between lightning fall-time (X, μs) (top panel), normalized peak
336 electric field (E, kV/m) (middle panel), and peak current (I, kA) (bottom panel) versus halo
337 diameters (W, km) for different types of sprites. The Pearson correlation coefficient (r) and
338 the linear fit equation (W, km) are denoted on the top corner of each panel.

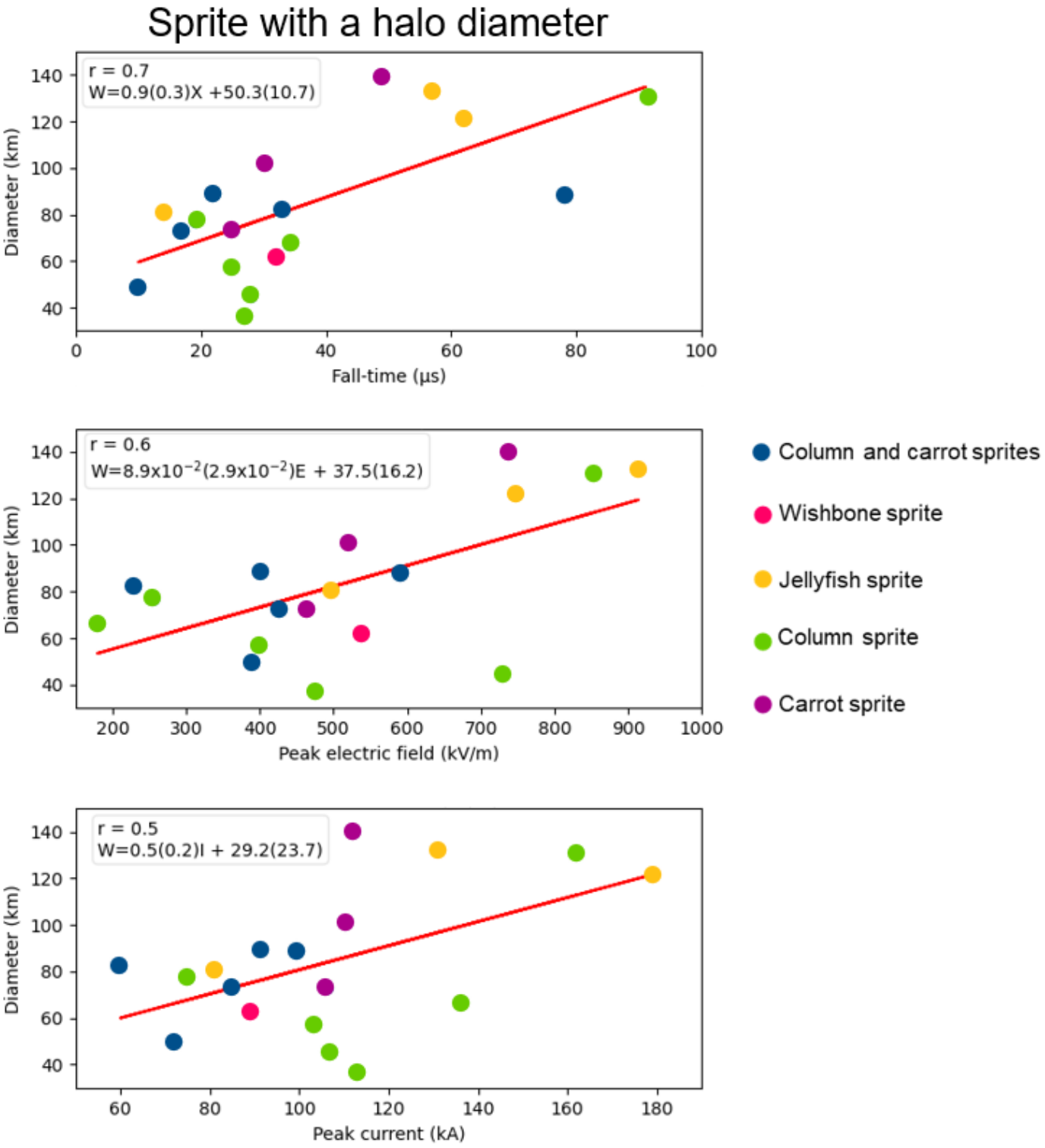

339

340 Fig. 4. Lightning fall-time (X, μs) (top panel), normalized peak electric field (E, kV/m) (middle panel), and peak
341 current (I, kA) (bottom panel) versus halo diameters (W, km) for different types of sprites (color-coded). Note

that the "column and carrot sprites" are where both types occur together. The Pearson correlation coefficient (r) and the linear fit equation (W, km) are denoted on the top corner of each panel. The value in parentheses in the linear fit equation is the uncertainty.

We found that halo diameters span between 37 and 140 km with an average of 84 (31) km, where the standard deviation is given in parentheses. A correlation coefficient of 0.7 exists between lightning fall-time and halo diameter, and a correlation coefficient of 0.6 exists between normalized lightning peak electric field and halo diameter. The lightning peak current and halo diameter show a good correlation (0.5), see Fig. 4. In all cases, the larger the lightning peak electric field, peak current, and fall-time, the larger the halo diameters.

A decrease in lightning parameter with altitude follows the behavior of the electric field and Maxwellian relaxation time in the Earth's atmosphere (Liu et al., 2015). It is known that the lightning CMC magnitude also depends on the duration of the continuing current. Thus, a longer continuing current enhances the lightning CMC magnitude estimate. The results suggest that the larger lightning CMC and fall-time are capable of sustaining maximum photon production at a low altitude compared to small lightning CMC and fall-time. The lightning CMC, peak electric field, peak current, rise-time and fall-time are essential in the generation and development of TLEs or sprite morphologies.

The results show that the lightning rise-time, fall-time, CMC, peak current, and peak electric field are essential in determining whether the lightning discharge initiated the TLEs or what type of sprite morphologies were initiated, especially for sprites with a halo. However, the results show that more than one lightning parameter is needed to determine the type of sprite morphology that was generated. The lightning rise-time, which is not usually reported (Asano et al., 2008; Haspel et al., 2020) and lightning fall-time, with no direct reports in the literature, should be included in the future lightning and TLEs studies.

Acknowledgments

DM thanks the South African National Space Agency and the University of KwaZulu-Natal for funding. DM, KM, and MF work was supported by the Royal Society (UK) grant NMG/R1/180252. JM acknowledges support from the National Science Centre, Poland, under grant 2015/19/B/ST10/01055. We thank Nickolay Ivchenko for operating the camera system from one of our observation sites.

References

Adachi, T., Fukunishi, H., Takahashi, Y. and Sato, M., 2004. Roles of the EMP and QE field in the generation of columniform sprites. *Geophys. Res. Lett*, *31*(4), L04107. https://doi.org/10.1029/2003GL019081

Asano, T., Hayakawa, M., Cho, M. and Suzuki, T., 2008. Computer simulations on the initiation and morphological difference of Japan winter and summer sprites. *J. Geophys. Res. Space Phys, 113*(A2). https://doi.org/10.1029/2007ja012528

Bering III, E. A., Benbrook, J. R., Bhusal, L., Garrett, J. A., Paredes, A. M., Wescott, E. M., ... and Lyons, W. A. 2004. Observations of transient luminous events (TLEs) associated with negative cloud to ground (− CG) lightning strokes. *Geophys. Res. Lett. 31*(5). https://doi.org/10.1029/2003gl018659

Bór, J. 2013. Optically perceptible characteristics of sprites observed in Central Europe in 2007–2009. *J. Atmos. Sol. Terr. Phys. 92*, 151-177. https://doi.org/10.1016/j.jastp.2012.10.008

Bór, J., Zelkó, Z., Hegedüs, T., Jäger, Z., Mlynarczyk, J., Popek, M. and Betz, H.D., 2018. On the series of +CG lightning strokes in dancing sprite events. *J. Geophys. Res. Atmos, 123*(19), pp.11-030. https://doi.org/10.1029/2017JD028251

Chen, A.B.C., Chen, H., Chuang, C.W., Cummer, S.A., Lu, G., Fang, H.K., Su, H.T. and Hsu, R.R., 2019. On negative sprites and the polarity paradox. *Geophys. Res. Lett. 46*(16), 9370-9378. https://doi.org/10.1029/2019gl083804

Cooray, V. and Lobato, A., 2020. The Energy, Momentum, and Peak Power Radiated by Negative Lightning Return Strokes. *Atmos. 11*(12), 1288. https://doi.org/10.3390/atmos11121288

Cummer, S.A., Inan, U.S., Bell, T.F. and Barrington-Leigh, C.P., 1998. ELF radiation produced by electrical currents in sprites. *Geophys. Res. Lett.*, *25*(8), pp.1281-1284. https://doi.org/10.1029/98GL50937

Earthnetworks.com. (2019). Sferic Maps [online] Available at: <https://www.earthnetworks.com/product/decision-support-collaboration-tools/sferic-maps/> [Accessed 01 February 2019]

Frey, H.U., Mende, S.B., Cummer, S.A., Li, J., Adachi, T., Fukunishi, H., Takahashi, Y., Chen, A.B., Hsu, R.R., Su, H.T. and Chang, Y.S., 2007. Halos generated by negative cloud-to-ground lightning. *Geophys. Res. Lett. 34*(18). https://doi.org/10.1029/2007gl030908

Füllekrug, M., Moudry, D.R., Dawes, G. and Sentman, D.D., 2001. Mesospheric sprite current triangulation. *J. Geophys Res. Atmos, 106*(D17), pp.20189-20194. https://doi.org/10.1029/2001JD900075

Füllekrug, M., Mareev, E.A. Rycroft, M.J. eds., 2006. Sprites, Elves and intense Lightning Discharges (Vol. 225). NATO Science Series II. Mathematics, physics and chemistry, Dordrecht: Springer, ISBN 1-4020-4628-630-42, 30-32. https://doi.org/10.1007/1-4020-4629-4

Füllekrug, M., 2010. Wideband digital low-frequency radio receiver. *Meas. Sci. Technol. 21*(1), 1-9. https://doi.org/10.1088/0957-0233/21/1/015901

Füllekrug, M., Nnadih, S., Soula, S et al., 2019. Maximum sprite streamer luminosity near the Stratopause. *Geophys. Res. Lett*. *46*(21), 12572-12579. https://doi.org/10.1029/2019GL084331

Gamerota, W.R., Cummer, S.A., Li, J., Stenbaek-Nielsen, H.C., Haaland, R.K. and McHarg, M.G., 2011. Comparison of sprite initiation altitudes between observations and models. *J. Geophys. Res. Space. Phys. 116*(A2). https://doi.org/10.1029/2010ja016095

Gijben, M., 2012. The lightning climatology of South Africa. *S. Afr. J. Sci*, *108*(3), 1-10. https://doi.org/10.4102/sajs.v108i3/4.740

Haspel, C., Tzabari, M. and Yair, Y., 2020. The influence of symmetric and non-symmetric charge configurations on the possibility of sprite inception: Numerical experiments with a 3D electrostatic model. *J. Atmos. Sol. Terr. Phys. 202*, 105245. https://doi.org/10.1016/j.jastp.2020.105245

Haspel, C., Kurtser, G. and Yair, Y., 2022. The feasibility of a 3D time-dependent model for predicting the area of possible sprite inception in the mesosphere based on an analytical solution to Poisson's equation. *J. Atmos. Sol. Terr. Phys, 230*, p.105853. https://doi.org/10.1016/j.jastp.2022.105853

Kulak, A. and Mlynarczyk, J., 2012. ELF propagation parameters for the ground-ionosphere waveguide with finite ground conductivity. *IEEE Trans. Antennas Propag., 61*(4), pp.2269-2275. http://dx.doi.org/10.1109/TAP.2012.2227445

Li, J., Cummer, S.A., Lyons, W.A. and Nelson, T.E., 2008. Coordinated analysis of delayed sprites with high-speed images and remote electromagnetic fields. *J. Geophys. Res. Atmos.* *113*(D20). https://doi.org/10.1029/2008JD010008

Liu, N., McHarg, M.G. and Stenbaek-Nielsen, H.C., 2015. High-altitude electrical discharges associated with thunderstorms and lightning. *J. Atmos. Sol. Terr. Phys. 136*, 98-118. https://doi.org/10.1016/j.jastp.2015.05.013

Liu, N., Boggs, L.D. and Cummer, S.A., 2016. Observation-constrained modeling of the ionospheric impact of negative sprites. *Geophys. Res. Lett. 43*(6), 2365-2373. https://doi.org/10.1002/2016gl068256

Luque, A. and Ebert, U., 2009. Emergence of sprite streamers from screening-ionization waves in the lower ionosphere. *Nat. Geosci. 2*(11), 757-760. https://doi.org/10.1038/ngeo662

Luque, A., Stenbaek-Nielsen, H.C., McHarg, M.G. and Haaland, R.K., 2016. Sprite beads and glows arising from the attachment instability in streamer channels. *J. Geophys. Res. Space. Phys. 121*(3), 2431-2449. https://doi.org/10.1002/2015ja022234

Malagón-Romero, A., Teunissen, J., Stenbaek-Nielsen, H.C., McHarg, M.G., Ebert, U. and Luque, A., 2020. On the emergence mechanism of carrot sprites. *Geophys. Res. Lett. 47*(1), e2019GL085776. https://doi.org/10.1029/2019gl085776

Mashao, D.C., Kosch, M.J., Bór, J et al., 2021. The altitude of sprites observed over South Africa. *S. Afr. J. Sci. 117*(1-2), 1-8. https://doi.org/10.17159/sajs.2021/7941

Mashao, D., Kosch, M., Fullekrug, M. and Ivchenko, M., 2022. 3D triangulation of Transient Luminous Events over Africa. *Adv. Space. Res*. https://doi.org/10.1016/j.asr.2022.08.057

McHarg, M.G., Haaland, R.K., Moudry, D. and Stenbaek-Nielsen, H.C., 2002. Altitude-time development of sprites. *J. Geophys. Res. Space Phys. 107*(A11), SIA-9. https://doi.org/10.1029/2001ja000283

McHarg, M.G., Stenbaek-Nielsen, H.C. and Kammae, T., 2007. Observations of streamer formation in sprites. *Geophys. Res. Lett. 34*(6), L06804. https://doi.org/10.1029/2006GL027854

Miyasato, R., Taylor, M.J., Fukunishi, H. and Stenbaek-Nielsen, H.C., 2002. Statistical characteristics of sprite halo events using coincident photometric and imaging data. *Geophys. Res. Lett. 29*(21), 29-1. https://doi.org/10.1029/2001gl014480

462 Mlynarczyk, J., Bór, J., Kulak, A., Popek, M. and Kubisz, J., 2015. An unusual sequence of
463 sprites followed by a secondary TLE: An analysis of ELF radio measurements and optical
464 observations. *J. Geophys. Res. Space Phys. 120*(3), 2241-2254.
465 https://doi.org/10.1002/2014ja020780

466 Mlynarczyk, J., Kulak, A., Klucjasz, S., Martynski, K., Kubisz, J. and Popek, M., 2018, May.
467 New broadband ELF receiver for studying atmospheric discharges in Central Europe. In *2018*
468 *Baltic URSI Symposium (URSI)* (pp. 155-157). IEEE.
469 https://doi.org/10.23919/ursi.2018.8406729

470 Nnadih, S., Kosch, M., Martinez, P. and Bor, J., 2018. First ground-based observations of
471 sprites over southern Africa. *S. A. J. Sci. 114*(9-10), 1-6.
472 https://doi.org/10.17159/sajs.2018/4272

473 Pasko, V.P., Inan, U.S., Bell, T.F. and Taranenko, Y.N., 1997. Sprites produced by quasi-
474 electrostatic heating and ionization in the lower ionosphere. *J. Geophys. Res. Space.*
475 *Phys*, *102*(A3), 4529-4561. https://doi.org/10.1029/96ja03528

476 Pasko, V.P., 2010. Recent advances in theory of transient luminous events. *J. Geophys. Res.*
477 *Space Phys. 115*(A6). https://doi.org/10.1029/2009ja014860

478 Pasko, V.P., Qin, J. and Celestin, S., 2013. Toward better understanding of sprite streamers:
479 initiation, morphology, and polarity asymmetry. *Surv. Geophys. 34*(6), 797-830.
480 https://doi.org/10.1007/s10712-013-9246-y

481 Peat, J., Barton, B. and Elliott, E., 2009. *Statistics workbook for evidence-based health care*.
482 John Wiley & Sons, 93-101. https://doi.org/10.1002/9781444300499
483 São Sabbas, F.T., Sentman, D.D., Wescott, E.M et al., 2003. Statistical analysis of space–
484 time relationships between sprites and lightning. *J. Atmos. Sol. Terr. Phys. 65*(5), 525-535.
485 https://doi.org/10.1016/S1364-6826(02)00326-7

486 Siingh, D., Singh, R.P., Singh, A.K., Kumar, S., Kulkarni, M.N. and Singh, A.K., 2012.
487 Discharges in the stratosphere and mesosphere. *Space sci. rev. 169*(1-4), 73-121.
488 https://doi.org/10.1007/s11214-012-9906-0

489 Stenbaek-Nielsen, H.C., Haaland, R., McHarg, M.G., Hensley, B.A. and Kanmae, T., 2010.
490 Sprite initiation altitude measured by triangulation. *J. Geophys. Res. Space Phys. 115*(A3).
491 https://doi.org/10.1029/2009ja014543

Soula, S., van der Velde, O., Montanyà, J., Neubert, T., Chanrion, O. and Ganot, M., 2009. Analysis of thunderstorm and lightning activity associated with sprites observed during the EuroSprite campaigns: Two case studies. *Atmos. Res. 91*(2-4), 514-528. https://doi.org/10.1016/j.atmosres.2008.06.017

Surkov, V.V. and Hayakawa, M., 2020. Progress in the study of transient luminous and atmospheric events: a review. *Surv. Geophys. 41*, 1101-1142. https://doi.org/10.1007/s10712-020-09597-2

Takahashi, Y., Yoshida, A., Sato, M., 2010. Absolute optical energy of sprites and its relationship to charge moment of parent lightning discharge based on measurement by ISUAL/AP. *J. Geophys. Res. Space. Phys., 115*(A9), A00E55. https://doi.org/10.1029/2009JA014814

Taylor, W.L. and Jean, A.G., 1959. Very-low-frequency radiation spectra of lightning discharges. NBS *J. Res. Radio Propagation D, 63*(2), 199. https://doi.org/10.6028/jres.063d.021

Taylor, M.J., Bailey, M.A., Pautet, P.D et al., 2008. Rare measurements of a sprite with halo event driven by a negative lightning discharge over Argentina. *Geophys. Res. Lett. 35*(14), L14812. https://doi.org/10.1029/2008GL033984

Vadislavsky, E., Yair, Y., Erlick, C., Price, C., Greenberg, E., Yaniv, R., Ziv, B., Reicher, N. and Devir, A., 2009. Indication for circular organization of column sprite elements associated with Eastern Mediterranean winter thunderstorms. *J. Atmos. Sol. Terr. Phys, 71*(17-18), pp.1835-1839. https://doi.org/10.1016/j.jastp.2009.07.001

Wang, Y., Lu, G., Ma, M et al., 2019. Triangulation of red sprites observed above a mesoscale convective system in North China. *Earth. Planet. Phys. 3*(2), 111-125. https://doi: 10.26464/epp2019015

Wescott, E.M., Sentman, D.D., Heavner, M.J et al., 1998. Observations of 'Columniform'sprites. *J. Atmos. Sol. Terr. Phys. 60*(7-9), 733-740. https://doi.org/10.1016/s1364-6826(98)00029-7

Wescott, E.M., Stenbaek-Nielsen, H.C., Sentman, D.D et al., 2001. Triangulation of sprites, associated halos and their possible relation to causative lightning and micrometeors. *J. Geophys. Res. Space Phys. 106*(A6), 10467-10477. https://doi.org/10.1029/2000ja000182

Williams, E., Kuo, C.L., Bór, J., Sátori, G., Newsome, R., Adachi, T., Boldi, R., Chen, A., Downes, E., Hsu, R.R. and Lyons, W., 2012. Resolution of the sprite polarity paradox: The role of halos. *Radio Sci. 47*(02), 1-12. https://doi.org/10.1029/2011rs004794

Yang, J., Lu, G., Liu, N., Sato, M., Feng, G., Wang, Y. and Chou, J.K., 2017. Sprite possibly produced by two distinct positive cloud-to-ground lightning flashes. *TAO: Terr. Atmos. Ocean. Sci. 28*(4), 609-624. https://doi.org/10.3319/tao.2016.07.22.01

Yaniv, R., Yair, Y., Price, C., Sato, M., Hobara, Y., Cummer, S., Li, J. and Devir, A., 2014. Ground-based observations of the relations between lightning charge-moment-change and the physical and optical properties of column sprites. *J. Atmos. Sol. Terr. Phys. 107*, 60-67. https://doi.org/10.1016/j.jastp.2013.10.018

Zhu, Y., Rakov, V.A., Tran, M.D et al., 2017. Evaluation of ENTLN performance characteristics based on the ground truth natural and rocket-triggered lightning data acquired in Florida. *J. Geophys. Res. Atmos. 122*(18), 9858-9866. https://doi.org/10.1002/2017JD027270

Appendix

Table 1. Summary of column and carrot sprites and sprites with halos including time, date, CG lightning strokes position and lightning peak current as reported by SAWS and EN; distance from the ELF receiver to the lightning location; lightning electric fields, rise-times, and fall-times computed from the ELF data; lightning CMC enumerated from the broadband magnetic field recording in the Bieszczady Mountains (49.20º N. 22.54º E), Poland; TLEs estimated top altitude, vertical extent, TLEs bottom altitude, and altitude of the brightest region; TLEs maximum brightness; number of TLEs elements and halo diameter. Different font color shows information related to sprites with halos (purple), column sprites (blue), and carrot sprites (black).

Time (UTC)	LAT (º)	LON (º)	Peak current (kA)	Distance from ELF receiver to lightning (km)	Electric field at 1 km from lightning location (kV/m)	Rise-time (µs)	Fall-time (µs)	CMC (C-km)	TLEs top altitude (km)	TLEs altitude of brightest region (km)	TLEs bottom altitude (km)	TLEs vertical extent (km)	TLEs maximum brightness (scaled brightness)	Number of TLEs elements	Halo diameter (km)
2019-02-01 18:45:10.752	-29.24	25.35	113	376.8	475.0	10	27	6090	72.7	65.5	36.0	36.74	116	1	37
2019-02-01 19:43:09.728	-29.60	25.07	103	333.4	396.6	11	25	2150	79.5	63.0	61.0	18.51	114	1	57
2019-02-01 20:10:11.537	-28.78	25.86	89	445.9	539.6	12	32	2130	75.6	60.2	38.0	37.59	251	2	63
2019-02-01 20:14:00.121	-29.71	25.29	60	347.3	229.3	8	33	3240	83.3	58.0	39.0	44.3	249	7	82
2019-02-01 20:29:36.130	-28.57	25.14	110	404.9	518.9	11	30	3790	80.5	58.5	47.6	32.9	253	4	102
2019-02-01 21:05:14.339	-29.24	24.62	75	319.1	255.8	22	19	689	82.3	56.6	52.4	29.97	150	1	77
2019-02-01 21:05:14.439	-29.05	24.78	72	344.3	388.8	10	10	3683	72.1	60.7	47.0	25.1	236	8	50
2019-02-01 21:18:40.722	-28.55	25.61	179	441.6	748.9	15	62	5270	86.0	65.0	45.0	40.97	254	12	122
2019-02-01 21:54:07.906	-28.90	26.63	131	504.4	914.0	8	57	6780	85.5	61.3	35.0	50.5	254	1	133
2019-02-02 20:54:36.370	-31.04	27.04	91	483.4	401.6	13	78	1340	79.9	51.4	33.0	46.87	230	4	89
2019-02-02 21:11:55.386	-30.25	26.58	99	448.6	592.4	16	22	2170	76.6	50.0	37.4	39.16	200	2	89

2019-02-02 22:44:38.719	-31.77	27.19	162	502.3	853.4	18	91	930	90.5	57.1	37.4	53.1	204	9	131
2019-02-11 19:53:57.116	-28.24	26.41	112	707.5	737.8	10	49	840	74.6	55.0	49.6	25	171	2	140
2019-01-30T20:40:17.642	-29.29	23.65	136	241.9	179.5	9	34	1620	81.2	64.0	42.6	38.6	220	2	67
2019-02-11 19:46:46.836	-28.22	25.66	107	656.1	727.2	8	28		83.3	68.0	58.4	24.9	225	9	45
2019-02-01 20:19:35.061	-29.02	25.34	106	389.1	463.5	10	25		71.5	59.0	35.0	36.5	251	1	73
2019-02-02 22:06:00.242	-31.18	26.98	81	476.7	496.6	25	14		73.6	57.0	33.5	40.1	241	4	81
2019-02-02 21:06:16.417	-30.96	27.19	85	496.4	425.8	14	17		72.0	50.0	32.0	40	251	10	73
2019-02-01 19:05:21.584	-29.38	25.21	50	357.3	355.4	10	19	2180	72.4	55.6	38.3	34.14	224	8	
2019-02-02 21:53:21.111	-31.15	27.02	50	481.0	293.6	7	30	2050	76.2	55.1	42.6	33.64	244	17	
2019-01-29 19:39:29.981	-29.42	24.39	34	289.1	100.8	12	20	1830	83.5	64.2	51.2	32.3	139	5	
2019-01-29 20:49:49.668	-29.23	24.79	56	332.7	173.7	16	4	2410	83.3	64.3	39.6	43.7	213	19	
2019-01-29 22:48:06.932	-28.18	24.71	44	406.4	203.1	10	1	1550	82.6	72.4	68.1	14.53	115	16	
2019-01-29 23:03:02.432	-28.13	24.69	34	410.2	192.0	11	21	2150	82.4	72.0	61.1	21.33	182	18	
2019-01-29T23:10:49.261	-27.91	24.32	51	421.3	181.1	10	19	1080	86.0	73.0	71.8	14.2	160	5	
2019-01-30T21:19:28.474	-29.34	24.82	87	328.0	274.3	11	11	880	79.8	71.3	66.0	13.8	111	3	
2019-01-30T22:05:21.758	-28.97	24.73	37	345.8	126.8	7	14	940	76.0	65.4	61.2	14.8	113	3	
2019-01-29 23:00:17.969	-28.20	25.06	36	428.9	197.6	15	14		86.4	71.8	66.1	20.3	123.0	14	
2019-02-01 19:24:25.922	-29.79	25.20	54	336.1	227.1	13	15		75.9	67.8	64.9	11	114.0	4	
2019-02-01 19:12:42.451	-29.86	25.41	62	351.5	301.0	17	4	2050	78.6	62.3	34.0	44.61	249	1	
2019-02-01 19:26:48.376	-29.56	25.04	41	332.9	179.6	8	13	1930	86.2	65.1	45.7	40.49	227	1	
2019-02-01 20:09:16.344	-29.62	25.20	66	344.2	369.6	6	30	3045	78.4	61.2	39.0	39.4	240	1	
2019-02-01 20:38:25.718	-28.61	25.53	68	431.1	427.4	8	32	2200	79.3	53.1	37.0	42.27	246	1	
2019-01-29 19:33:50.302	-29.40	24.33	50	285.2	124.0	19	24	1360	83.7	66.0	52.3	31.4	198	6	
2019-01-29 20:25:41.984	-29.51	25.18	38	347.6	144.7	8	1	3060	85.0	62.0	41.0	44	241	6	
2019-01-29 20:38:40.528	-29.45	25.18	67	350.6	148.2	11	1	2160	87.0	62.0	33.8	53.2	246	10	
2019-01-29 19:17:59.218	-30.13	24.35	70	245.9	93.3	19	1	1680	83.3	68.5	37.0	46.3	247	12	
2019-02-01 19:55:34.857	-29.35	25.44	52	378.3	204.7	9	25		74.1	57.9	32.3	41.8	228	1	
2019-02-01 20:15:43.526	-29.02	25.32	92	387.6	425.3	7	25		70.7	50.0	32.0	38.65	253.0	1	
2019-02-01 19:24:26.151	-30.05	24.90	32	297.8	146.4	9	16		80.8	62.7	31.0	49.8	251.0	3	

557